Physics and Chemistry of Minerals (2021) 48:4
https://doi.org/10.1007/s00269-020-01131-5

ORIGINAL PAPER

Crystal–fluid interaction: the evolution of stilbite structure at high pressure

Yu. V. Seryotkin[1,2] · S. N. Dementiev[1] · A. Yu. Likhacheva[1,2]

Received: 29 September 2020 / Accepted: 9 December 2020 / Published online: 11 January 2021

Abstract

Natural stilbite, $Ca_{4.00}Na_{1.47}(H_2O)_{30}[Al_{9.47}Si_{26.53}O_{72}]$, space group $F2/m$, $a = 13.5978(3)$, $b = 18.2804(4)$, $c = 17.8076(4)$ Å, $\beta = 90.685(2)°$, $V = 4426.18(17)$ Å^3, $Z = 2$, has been studied by single-crystal X-ray diffraction method at ambient conditions and under compression in penetrating (water-bearing) and non-penetrating (paraffin) media. In water-containing medium during the first compression stage (below 1 GPa) the pressure-induced hydration effect manifests in the additional occupation of partly vacant H_2O positions; above 1 GPa the H_2O position, which is vacant at ambient pressure and not linked to cations, becomes occupied. Above 2.6 GPa the composition of stilbite remains almost constant; apparently no further hydration is possible. The compressibility of stilbite in paraffin is expectedly higher compared to that in penetrating medium. The cations coordination changes mainly through minor shifts of water positions and some re-distribution of their occupancy. Above 3 GPa the structure abruptly contracts along the *b* axis; the structure symmetry is reduced to triclinic. The decompression experiments show full reversibility of structural changes on pressure release.

Keywords Stilbite · Single-crystal X-ray diffraction · High pressure · Crystal–fluid interaction · Structure evolution

Introduction

The microporous compounds, such as zeolites, possess a system of channels and cavities, whose dimensions allow the diffusion of molecules and cations under the interaction with the external medium. This favors an easy exchange of the extra-framework cations (Pabalan and Bertetti 2001), as well as (for several zeolites) variations of the H_2O content in the structure voids, depending on the external conditions. Molecular-sieve properties of zeolites lead to a variable behavior of these substances at hydrostatic compression, depending on the nature of the pressure-transmitting medium. The compression medium can be "penetrating" (whose molecules can enter the structure channels due to steric reasons) or "non-penetrating". In the first case the crystal–fluid interaction and, correspondingly, the penetration of additional H_2O molecules in zeolite channels is possible. Therefore, additional H_2O molecules can enter the channels on compression in water-containing medium (pressure-induced hydration (Lee et al. 2001)—PIH). In some zeolites (Lee et al. 2002; Arletti et al. 2010), such overhydration occurs under the compression in the so-called "nominally penetrating medium"—methanol:ethanol:water mixture with a volume ratio of 16:3:1. In contrast, there is no overhydration in phillipsite (Gatta and Lee 2007) and thomsonite (Lee et al. 2004) compressed in "nominally penetrating medium", whereas thomsonite, compressed in the ethanol:water 1:3 mixture, transformed at 2 GPa into a new phase with high water content (Likhacheva et al. 2007). This example shows that the relative content of water in the hydrostatic medium is of particular importance. The PIH effect is controlled by several variables (Gatta et al. 2018): "free diameter" of the framework cavities, chemical nature and configuration of the extra-framework population, partial pressure of the penetrating molecule in the fluid (for example, $P(H_2O)$ in a methanol–ethanol–water 16:3:1 mixture), the temperature at which the experiment is conducted. The

Supplementary Information The online version contains supplementary material available at https://doi.org/10.1007/s00269-020-01131-5.

✉ Yu. V. Seryotkin
yuvs@igm.nsc.ru

[1] V.S. Sobolev Institute of Geology and Mineralogy, Siberian Branch of Russian Academy of Sciences, Novosibirsk, Russia

[2] Novosibirsk State University, Novosibirsk, Russia

diffusion mobility of the H_2O molecules in the channels is also an important factor, which depends on the character of H_2O–framework and H_2O–H_2O bonds, as well as on the defectiveness of the extra-framework subsystem (presence/absence of vacancies).

Zeolites of stilbite–stellerite group $|Ca_4Na_n(H_2O)_m|[Al_{8+n}Si_{28-n}O_{72}]$, $0 \le n \le 2$, are characterized by variable composition and statistical occupation of the extra-framework sites in their channels. The H_2O molecules are located in the large cavity around the Ca atom; the number of water sites with the occupancy of 0.13–1.00 varies from six to eleven (Slaughter 1970; Galli 1971; Quartieri and Vezzalini 1987; Drebushchak et al. 2012). These peculiarities of the extra-framework subsystem of zeolites belonging to stilbite group determine their high molecular self-diffusion (Dyer and Faghihian 1998; Xu and Stebbins 1998).

Variable composition of zeolites of stilbite group and the presence of vacant sites, which are potentially suitable for filling with the H_2O molecules, stipulates its study under high pressure. The compressibility of stilbite in water-containing medium was characterized by X-ray powder diffraction (Seryotkin et al. 2012), however the peculiarities of its structural evolution were not studied. Our aim is to study the evolution of stilbite structure under the compression in penetrating and non-penetrating medium.

Experimental

The stilbite crystals (Nizhnyaya Tunguska region, East Siberia) with composition $Ca_{4.00}Na_{1.47}(H_2O)_{30}\cdot[Al_{9.47}Si_{26.53}O_{72}]$ (Seryotkin et al. 2012) were provided by Igor A. Belitsky. Several pieces of a large crystal were first checked under a polarizing microscope for the absence of twinning, and a $0.14 \times 0.10 \times 0.03$ mm tabular fragment was selected for the single-crystal X-ray diffraction measurements. Diffraction data were initially collected at ambient conditions on an Oxford Diffraction Xcalibur Gemini diffractometer (MoKα radiation, 0.5 mm collimator, graphite monochromator, ω scan with the step of 1°, 60 s per frame). Data reduction, including the background correction and Lorentz and polarization corrections, was accomplished with the *CrysAlis Pro* 171.37.35 program package (Rigaku Oxford Diffraction 2016). Multi-scan technique was used for a semi-empirical absorption correction. The structure was solved and refined using SHELX-97 program package (Sheldrick 2015). The Si/(Al + Si) ratio for each tetrahedral site was estimated according to the method proposed by Koyama and Takeuchi (1977). All atoms excluding low-populated Na and Ow6 positions were refined in anisotropic approximation.

The same fragment was used for the high-pressure experiments in a Boehler–Almax diamond–anvil cell (DAC) (Boehler 2006) (0.200 mm stainless steel gasket pre-indented to 0.110 mm, 0.3 mm diameter hole). The pressure value was determined with the accuracy of ± 0.05 GPa using ruby as a luminescence pressure sensor (Piermarini et al. 1975). An ethanol–water (4:1) mixture was employed as a pressure-transmitting medium in the first experimental series. Single-crystal diffraction measurements were performed at 7 pressure points in the range of 0.26–4.25 GPa (Table 1). The ω scan technique was used for data collection, with a scan step of 0.5° and a time of 90 s per frame, according to the strategy of *CrysAlis Pro* applied for high-pressure measurements in DAC.

After the first experimental series, DAC was released to ambient pressure, opened and dried to clear the sample chamber from ethanol–water liquid. Then the DAC chamber was loaded with paraffin, which is used as a non-penetrating medium. The second series of diffraction measurements (6 pressure points) was performed with the crystal and experimental parameters identical to those used in the first series. In addition, the data for the two pressure points were collected on decompression (See Table 1).

The high-pressure diffraction data were reduced with *CrysAlis Pro* software as from a single crystal, excluding the diamond reflections. In the experiment with water-containing medium, the peaks of ice emerged above 2 GPa. The overlay of the peaks of the sample and diamond/ice was monitored manually and the peaks belonging to more than one phase were eliminated. The absorption by diamonds, the gasket and the crystal was corrected numerically with Absorb-7 software (Angel and Gonzalez-Platas 2013). The structures were refined using SHELX-97 program package; the structural parameters obtained for the previous pressure point were set as the starting model.

After the high-pressure experiment, the sample was withdrawn from the DAC, and the diffraction measurements were performed to assess the reversibility of pressure-induced changes in the stilbite structure.

The pressure dependences of the unit-cell parameters of stilbite structure are presented in Table 1. The experimental details for the data collection and structure determination are listed in Tables 2 and 3. The results of structural refinement are presented in Supplementary materials (Tables S1, S2, S3, S4, S5, S6, CIF files).

Results and discussion

Structure of stilbite at ambient conditions

The tetrahedral framework of topological type STI is based on heulandite secondary building unit (SBU) 4–4=1. The framework is characterized by a pronounced sub-layered structure; the layer is composed of only four-, five- and six-membered rings, which prohibit the diffusion of

Table 1 Lattice parameters and volumes of stilbite at high pressure

P, GPa	*a*, Å	*b*, Å	*c*, Å	*α*, °	*β*, °	*γ*, °	*V*, Å^3
0.0001	13.5978 (3)	18.2804 (4)	17.8076 (4)	90	90.685 (2)	90	4426.18 (17)
Compression in ethanol:water 4:1							
0.26	13.5702 (3)	18.287 (3)	17.7758 (4)	90.027 (5)	90.7952 (18)	90.050 (5)	4410.7 (7)
0.81	13.5176 (3)	18.195 (2)	17.6899 (3)	89.971 (4)	91.0133 (16)	90.061 (5)	4350.3 (5)
1.37	13.4872 (3)	18.142 (2)	17.5996 (4)	90.023 (5)	91.1845 (17)	90.036 (5)	4305.4 (5)
2.02	13.4609 (3)	18.076 (2)	17.5106 (4)	89.995 (5)	91.3426 (17)	90.029 (5)	4259.6 (5)
2.65	13.4178 (3)	18.026 (2)	17.4090 (4)	89.998 (5)	91.4417 (17)	90.026 (5)	4209.3 (5)
3.40	13.3663 (3)	17.9091 (18)	17.3009 (4)	89.784 (5)	91.4476 (18)	90.188 (4)	4140.1 (4)
4.25	13.3200 (5)	17.792 (3)	17.1775 (5)	89.366 (8)	91.395 (3)	90.477 (8)	4069.3 (7)
Compression in paraffin							
0.10	13.5860 (3)	18.2755 (18)	17.7947 (4)	90.041 (5)	90.7311 (19)	90.043 (5)	4417.9 (5)
0.84	13.4975 (3)	18.1638 (18)	17.6420 (4)	90.013 (5)	91.0524 (19)	90.035 (5)	4324.5 (5)
1.82	13.3914 (3)	18.0211 (16)	17.4400 (4)	90.218 (4)	91.3176 (17)	89.893 (4)	4207.6 (4)
2.82	13.3031 (6)	17.914 (2)	17.2803 (6)	90.357 (8)	91.463 (3)	89.727 (9)	4116.6 (5)
3.85	13.2564 (12)	17.584 (12)	16.988 (7)	90.84 (6)	91.366 (17)	89.40 (2)	3958 (3)
4.95	13.2418 (8)	17.446 (6)	16.5677 (14)	90.427 (18)	90.972 (6)	88.976 (15)	3826 (1)
3.35*	13.2792 (7)	17.878 (4)	17.1567 (15)	90.534 (19)	91.413 (6)	89.337 (11)	4071 (1)
2.48*	13.3353 (9)	17.979 (3)	17.2827 (10)	90.245 (12)	91.537 (5)	89.804 (12)	4142.1 (8)
0.0001#	13.5964 (3)	18.2783 (5)	17.7982 (4)	90	90.729 (2)	90	4422.8 (2)

*Data measured on decompression

#After decompression, in air

Table 2 Parameters of data collection and structure refinement for stilbite compressed in penetrating medium

Pressure (GPa)	0.0001	0.26	0.81	1.37	2.02	2.65	3.40
Space group	*F*2/*m*	*F*2/*m*	*F*2/*m*	*F*2/*m*	*F*2/*m*	*F*2/*m*	*F*2/*m*
d (g/cm^3)	2.180	2.202	2.239	2.268	2.305	2.333	2.372
μ (MoKα) (/mm)	0.864	0.868	0.881	0.891	0.902	0.913	0.928
Scan width (°/frame)	1	0.5	0.5	0.5	0.5	0.5	0.5
Exposure (s/frame)	60	90	90	90	90	90	90
2*θ* range (°)	4.36–63.57	4.36–63.62	4.38–63.45	4.38–63.75	4.40–63.90	4.41–63.33	4.42–62.98
Number of I_{hkl} measured	22,999	9687	9575	9493	9417	9294	8917
Number of unique F^2_{hkl}	3780	1060	1038	1028	1019	1005	987
R_{int}	0.0709	0.0890	0.0874	0.0931	0.0967	0.0882	0.1195
Reflections with $I > 2\sigma(I)$	2814	784	791	769	751	754	715
Number of variables	252	177	183	175	167	176	176
*R*1, *wR*2 for observed reflections [$I > 2\sigma I$]	0.0494, 0.1030	0.0516, 0.1200	0.0505, 0.1175	0.0500, 0.1167	0.0497, 0.1147	0.0486, 0.1096	0.0606, 0.1283
*R*1, *wR*2 for all data	0.0759, 0.1150	0.0767, 0.1333	0.0709, 0.1281	0.0746, 0.1304	0.0756, 0.1284	0.0723, 0.1218	0.0958, 0.1452
GooF	1.049	1.032	1.065	1.050	1.071	1.048	1.118
Residual electron density (*e*/Å^3)	0.624, − 0.584	0.364, − 0.571	0.432, − 0.438	0.398, − 0.359	0.438, − 0.315	0.469, − 0.365	0.447, − 0.390

cations and H_2O molecules. The layers joints form two-dimensional system of large channels with the aperture of 10-membered rings along the *a* axis and two types of 8-membered rings alternating in the channel along the *c* axis (Fig. 1a, b). The topological symmetry of the framework *Fmmm* is realized in stellerite structure [idealized composition $|Ca_4(H_2O)_{28}|[Al_8Si_{28}O_{72}]$ (Gottardi and Galli 1985)—sodium-free member of stilbite group. Depending on the composition, the symmetry of the other members of stilbite group is lowered to *F*2/*m* (proper

Table 3 Parameters of data collection and structure refinement for stilbite compressed in paraffin

Pressure (GPa)	0.10	0.84	1.82	2.82	0.0001*
Space group	*F*2/*m*	*F*2/*m*	*F*2/*m*	*F*2/*m*	*F*2/*m*
d (g/cm^3)	2.184	2.231	2.293	2.344	2.182
μ (MoKα) (/mm^{-1})	0.865	0.884	0.908	0.928	0.864
Scan width (°/frame)	0.5	0.5	0.5	0.5	1.0
Exposure (s/frame)	90	90	90	90	60
2θ range (°)	4.36–63.31	4.38–63.44	4.41–63.27	4.43–63.39	4.36–63.61
Number of I_{hkl} measured	9584	9421	9059	8673	22,772
Number of unique F^2_{hkl}	1081	1059	1033	997	3796
R_{int}	0.1112	0.1068	0.1225	0.1523	0.0744
Reflections with $I > 2\sigma(I)$	733	750	712	640	2746
Number of variables	182	189	191	182	247
$R1$, $wR2$ for observed reflections [$I > 2\sigma I$]	0.0630, 0.1464	0.0527, 0.1198	0.0532, 0.1114	0.0674, 0.1324	0.0497, 0.1018
$R1$, $wR2$ for all data	0.0993, 0.1700	0.0854, 0.1350	0.0893, 0.1280	0.1153, 0.1536	0.0803, 0.1145
GooF	1.034	1.099	1.104	1.112	1.046
Residual electron density (e/Å^3)	0.388, − 0.490	0.360, − 0.327	0.353, − 0.484	0.637, − 0.429	0.654, − 0.762

*After decompression, in air

stilbite) or *Amma* (barrerite, Na, K-variety). All members are Si, Al disordered (Gottardi and Galli 1985).

The extra-framework cations can occupy four different sites—*A*, *B*, *C*, and *D* (Fig. 1d). The schematic positional formula is $A_4B_4C_2D_2(H_2O)_{30}[T_{36}O_{72}]$, $Z = 2$. These positions are ascribed to cations by Slaughter (1970). The *A* site (Ca, Na in the notation of Slaughter (1970)) resides in a large cavity on the channels joint; its cation has no contacts with the framework O atoms and is coordinated only by the H_2O molecules. The *B* site (Na(1)) lies in the plane of 10-membered ring 10mR[100] (Fig. 1a) between the two *A* sites. Its coordination includes, besides the H_2O molecules, two to four framework O atoms. The *C* site (X) resides in the 8-membered ring 8mR[001]C (Fig. 1b) at the channels boundary and is coordinated by four framework oxygens and 3–4 H_2O molecules. The *D* site (Na(2) and Na(3)) lies in the 8-membered ring 8mR[001]D (Fig. 1b) also at the channels boundary. Depending on the cation type, its coordination can include 2–8 framework O atoms and 1–2 H_2O molecules. As a rule, in stilbite structure only two positions are occupied (Armbruster and Gunter 2001): the Ca^{2+} cations are in the *A* sites and Na^+ are located in one of the two subsystems of the B sites, which are differentiated due to symmetry reduction with respect to the topological symmetry. In the structure of K,Na-substituted stellerite, the cations occupy the positions *B*, *C* and *D*; the *A* sites are vacant (Seryotkin and Bakakin 2019).

A fragment of stilbite structure at ambient conditions is presented in Fig. 2a. The Ca^{2+} cations lie in the center of a large cavity on the channels joint (*A* site). The H_2O molecules occupy 21 positions near Ca; their occupancy varies from 0.03 to 0.71. This adds up to 7.8 water molecules in Ca coordination. The Na^+ cations are traditionally located in the *B*1 sites with the occupancy 0.10. Their coordination (within 2.36–2.98 Å) includes two framework O-atoms and five H_2O positions with a total occupancy of 2.08(4) molecules.

Compression of stilbite in water-containing medium

During the first stage of stilbite compression in penetrating medium (below 1 GPa) the PIH (pressure-induced hydration) effect is manifested by additional filling of the partly vacant H_2O positions (Fig. 3); the total H_2O content increases by 1.7 molecules p.f.u. (Table 4). Interestingly, at that the number of split positions decreases: for example, the Ca coordination changes from 21 sites at ambient conditions to 17 sites at 0.81 GPa, the total H_2O content being increased from 7.8 to 8.2 molecules (ESD = 0.2 H_2O molecules). The changes in the Na coordination consist of a minor re-distribution of the H_2O molecules between the neighbor positions, their total occupancy (2.00(6) H_2O molecules) being preserved.

Above 1 GPa a vacant (at ambient conditions) H_2O site Ow8, located near the center of the 8mR[100]D ring out of the cations coordination, becomes occupied (Fig. 2b). The total amount of the H_2O molecules in the Ca coordination remains constant (8.1–8.2 with ESD = 0.2) above 1 GPa, i.e. the additional hydration within this pressure range is fully determined by the increase of the Ow8 occupancy (Fig. 3). At 2.65 GPa it makes 0.49(2), which corresponds to the increase of the total H_2O content by two more molecules p.f.u. (see Table 4). Above 2.65 GPa the composition of stilbite practically does not change. In the vicinity of Ow8 the symmetrically multiplied site Ow8 and a half occupied

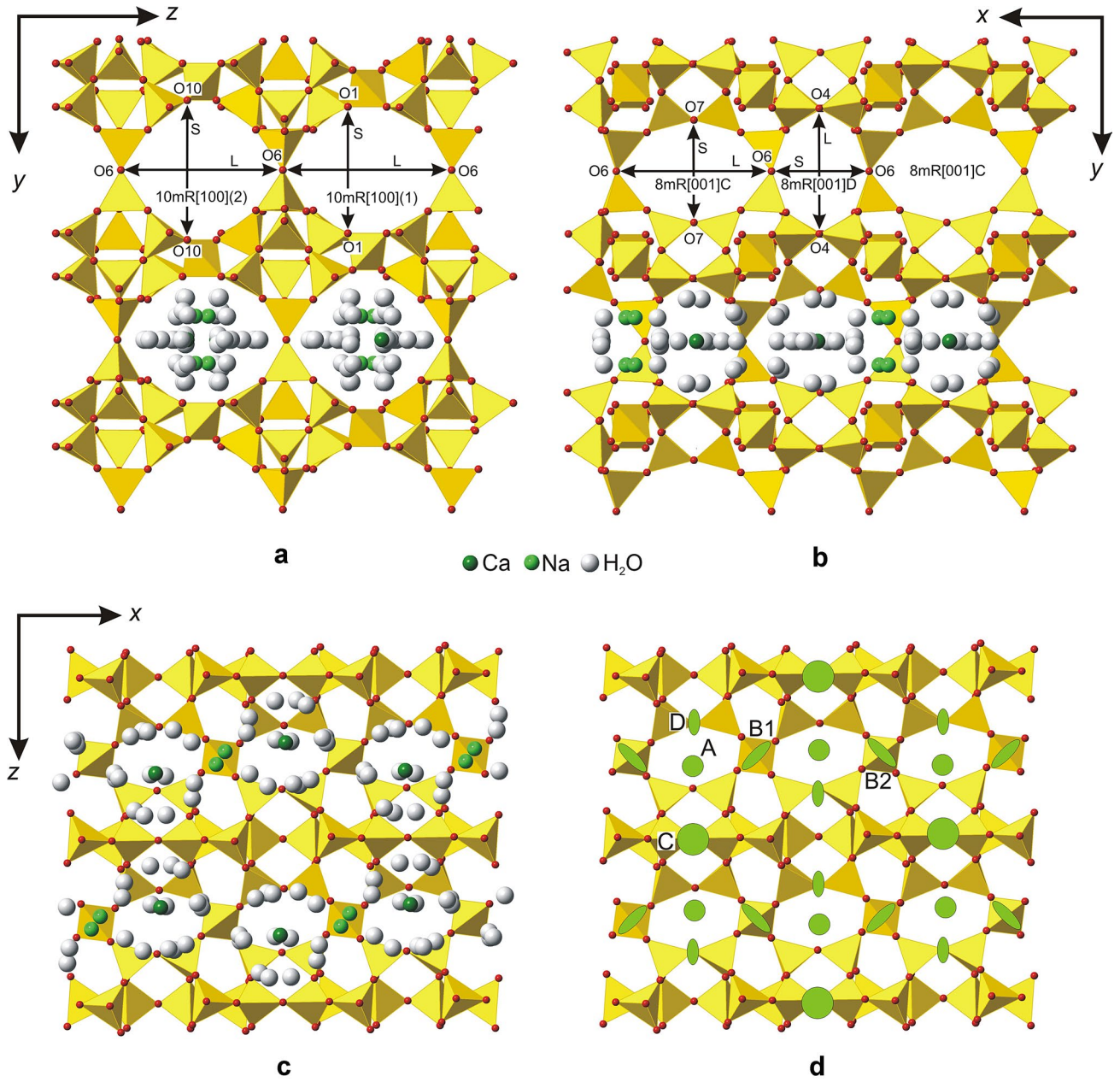

Fig. 1 Stilbite structure in projection along [100] (**a**), [001] (**b**) and [010] (**c**). The scheme of cation sites in the structure of STI topology (**d**); sites *B* and *D* are shown as ellipses due to statistical shift of the atoms. The ellipticity ε of the channels of 10-(10mR[100](1) and 10mR[100](2)) and 8-membered (8mR[001]C and 8mR[001]D) rings is defined by a ratio of the smaller (*S*) and the larger (*L*) channel diameter: $\varepsilon = S/L$ (Lotti et al. 2015)

Ow5 are located at short distances (1.9 and 2.4 Å, respectively). Therefore, the Ow8 cannot be filled more than half. Hence, above 2.65 GPa there is no more possibility for the additional hydration.

A gradual increase of the water content in stilbite structure with pressure, evidently, is caused by the rise of partial water pressure in compressing medium. Note that many zeolites behave similarly at normal conditions, as well as during their compression in penetrating medium. For example, the water content in the structure of large-pore zeolites of heulandite–clinoptilolite group can increase by one third under the change of the air humidity (Carey and Bish 1996). Under the compression in water-bearing medium their H_2O content also increases in a large pressure range (Seryotkin 2015, 2016). Laumontite demonstrates a similar behaviour (Fridriksson et al. 2003; Rashchenko et al. 2012a, b). Such behaviour is related with a developed self-diffusion of the H_2O molecules in the framework channels (Barrer and Fender

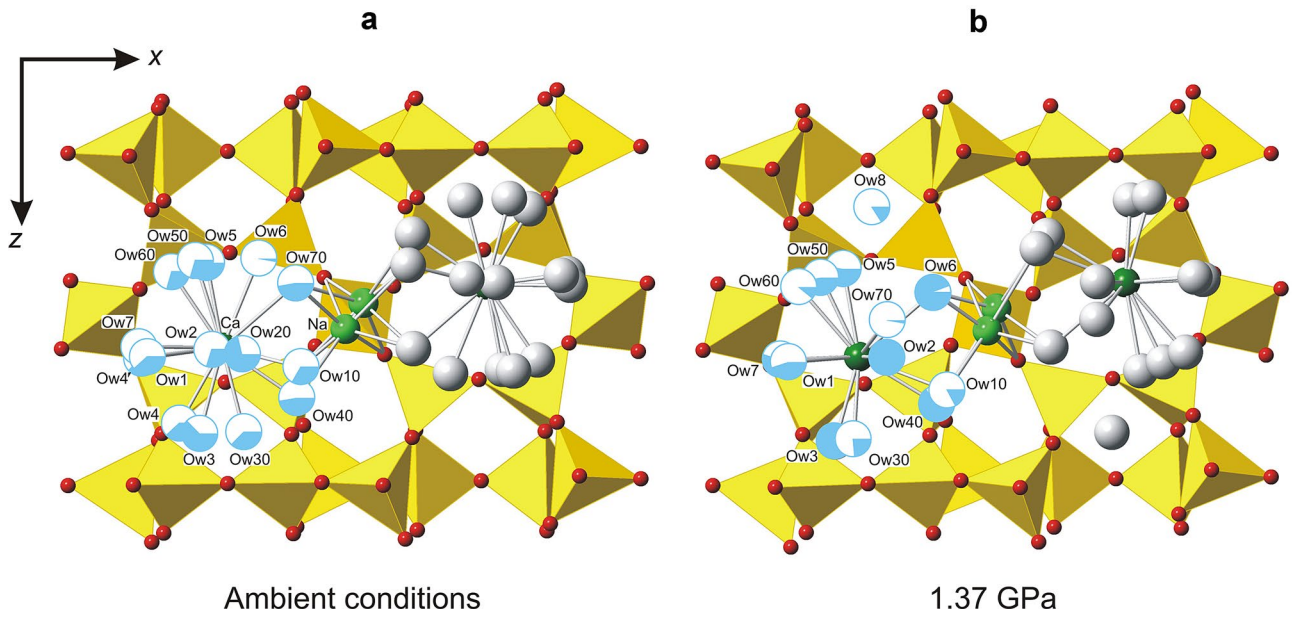

Fig. 2 The fragment of stilbite structure in projection along the *c* axis at ambient conditions and at 1.37 GPa. The Ow sites occupancy is indicated on the left

1961; Gabuda and Kozlova 1995), which implies the interaction with the external medium and respective molecular exchange. The authors have no information about the works devoted to the influence of the air humidity onto the H_2O content in stilbite, however, the studies of the H_2O self-diffusion in stilbite structure (Dyer and Faghihian 1998) evidence for high mobility of the H_2O molecules at ambient conditions. This implies also the influence of partial water pressure in the external medium onto the H_2O content in stilbite.

Upon the pressure increase the number of split water positions keeps decreasing, which is evidently related to the volume reduction of the large cages hosting the water-cation assemblages $Ca(H_2O)_8$. Namely, at 2.65 GPa the Ca coordination includes only 14 water sites containing 8.1(2) H_2O molecules. Taking into consideration the constant H_2O content of the Ca coordination, one can assert that the decrease of the number of split sites is accompanied by the redistribution of the occupancy of the remaining sites. The Na positions, on the contrary, acquire additional ligands through the shift of the Ow6 sites towards them; at that, however, their total occupancy remains close to two molecules.

It is interesting to examine how the distances Ca–Ca and Ca–Na in the triads A–B1–A and A–B2(vacancy)–A change with pressure. In the course of additional hydration (ambient conditions—2.65 GPa) the distance Ca–Ca in the triad A–B1–A increases regularly from 7.28 to 7.58 Å with simultaneous increase of the distance Ca–Na (from 3.57 to 3.67 Å), and only in the range of constant composition (above 3 GPa) these distances decrease. On the contrary, in the triad A–vacancy–A the distance Ca–Ca decreases regularly from 6.69 Å at normal conditions to 6.40 Å at 2.65 GPa.

Above 3 GPa the unit cell metrics becomes triclinic, and the distortion increases with pressure. The structure refinement in monoclinic approximation at 3.40 GPa gives reasonable results, but at 4.25 GPa the refinement factors and structure characteristics of the monoclinic model are unsatisfactory. The collected diffraction data are insufficient to refine triclinic structure due to a restricted angular range of diffraction measurements in DAC.

Within the whole studied range, the pressure dependence of the unit cell volume is close to linear and has no anomalies, including the pressure range where the composition becomes constant (Fig. 4). Within this range the $a(P)$ and $b(P)$ curves (Fig. 4) exhibit a slight increase of the compressibility; the *c* parameter decreases almost linearly with pressure.

Upon the pressure increase from ambient conditions to 3.4 GPa the framework T–O–T angles change from − 8.0° (T1–O1–T4) to 8.4° (T10–O20–T3), averaging − 2.3°. Such a significant increase of the T10–O20–T3 angle is related with a large deformation of the 4-membered rings forming SBU, involving also the decrease of the T1–O2–T3 angle in the same ring by 8.2°. In the structure of monoclinic stilbite, the 10-membered rings differentiate into two types, and their aperture is determined by the distances O1–O1 and O10–O10. Therefore, a significant decrease of the T1–O1–T4 angle corresponds to the diminishing of O1–O1 distance and, respectively, the increase of the ellipticity of the ring 10mR[100](1) (Fig. 5). In this case, the ellipticity

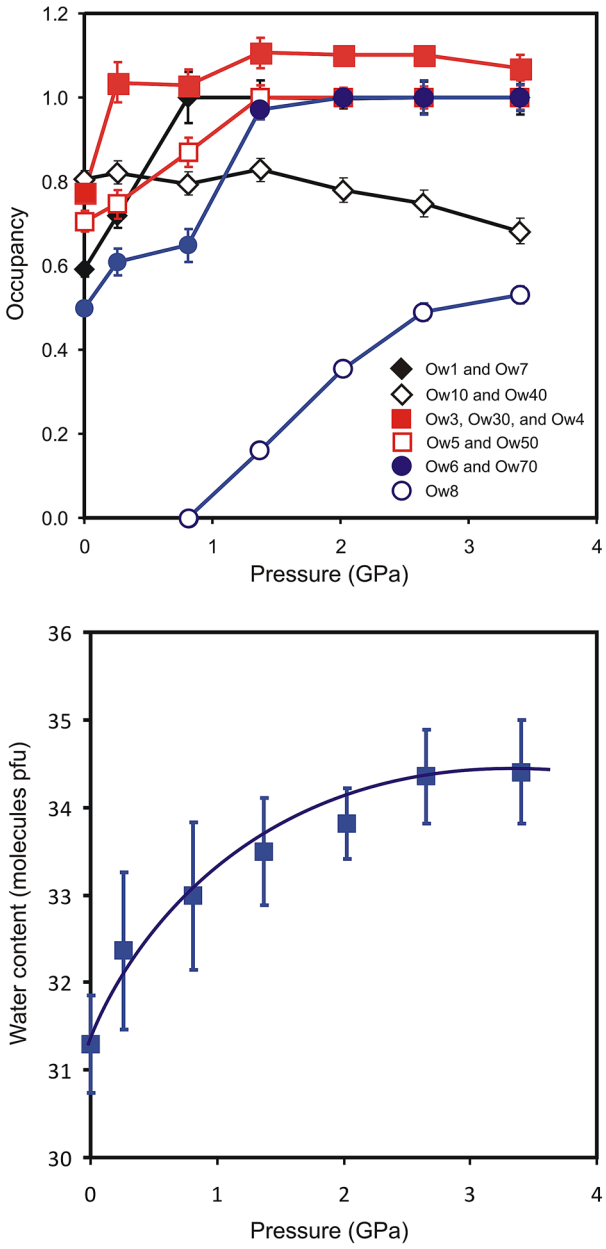

Fig. 3 The change of the H_2O content in stilbite upon the compression in penetrating medium. The total occupancy of the nearest (< 2 Å) water positions is indicated at the top. The number of the H_2O molecules p.f.u. is given at the bottom

is determined by the ratio of a smaller to a larger diameter of the channel: $\varepsilon = S/L$ (Lotti et al. 2015). In the absence of ellipticity, this value is equal to one, and the increase of ellipticity leads to the ε diminishing. Though the T10–O10–T4 angle is also reduced, even to a lesser value (−4.2°), the ellipticity of the ring 10mR[100](2) decreases with pressure, also due to the contraction of the ring 10mR[100](1). Moreover, distance O10–O10 regularly increases during compression (Table 5). Note that there is Na site in the plane of 10mR[100](1); we can suppose that the framework linked to the water-cation assemblage $Na(H_2O)_n$ experiences its "form-building" influence.

Table 4 The change of the water content in stilbite compressed in penetrating medium

Pressure, GPa	Number of H_2O molecules, p.f.u.
0.0001	31.3 (6)
0.26	32.4 (10)
0.81	33.0 (8)
1.37	33.5 (6)
2.02	33.8 (4)
2.65	34.4 (5)
3.40	34.4 (6)

The decrease of the distance O1–O1 (see Table 5) determining the aperture of the ring 10mR[100](1) is accompanied by a regular decrease of the occupancy of the H_2O sites Ow10 and Ow4, which are situated near the ring (Fig. 3) and enter the Na coordination. The position Ow70, which also belongs to the Na coordination, is initially half occupied. Already at 1.37 GPa its occupancy decreases to 3%, and upon the further pressure increase it remains vacant.

The ellipticity of the ring 8mR[001]C is almost constant within the whole pressure range, whereas the ring 8mR[001]D becomes more isometric above 1 GPa, evidently due to the occupation of a new water site near the ring center. The ellipticity continues to decrease even at constant composition, but this is determined by a larger contraction of the ring along its greater diameter (*y* axis).

Compression of stilbite in paraffin

Within 3 GPa the compressibility of stilbite in paraffin is considerably higher compared to that in penetrating medium only along the *a* axis (Fig. 3); the dependences $b(P)$ and $c(P)$ for both media are similar. The changes in the cations coordination consist only in small shifts of the water positions and some re-distribution of their occupancy. Interestingly, the pressure dependencies of the ellipticity of 10-membered rings are almost identical for both media. This is not true for the 8-membered rings. For example, upon the compression in paraffin the ellipticity of both rings undergoes minor but distinct increase (Table 6).

Above 3 GPa the structure contracts abruptly (probably stepwise) along the *b* axis; in the two other directions the changes are almost regular (Fig. 3). The structure symmetry is reduced to triclinic.

The decompression experiments have shown full reversibility of structural changes on pressure release (Fig. 3).

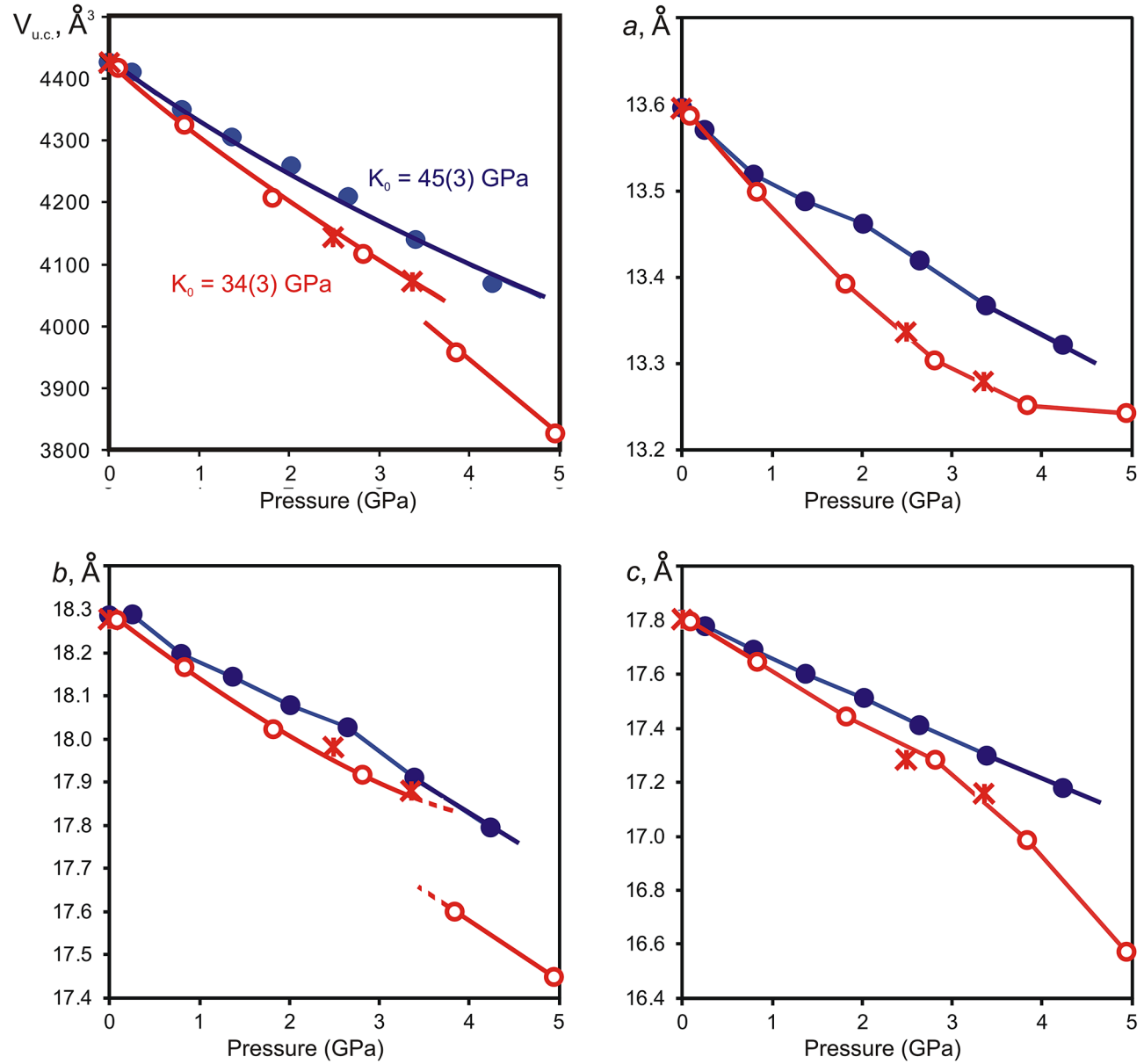

Fig. 4 Unit-cell parameters of stilbite upon the compression in penetrating (filled symbols) and non-penetrating (open symbols) media. Asterisks mark the values measured for stilbite compressed in paraffin on the pressure release

Volume compression data for both experimental series were fitted to a two-order Birch–Murnaghan equation of state using EoSFit 7.10 program (Angel et al. 2014). For the sample compressed in water–ethanol mixture, the refined values of V_0 and K_0 are 4426.19(17) Å^3 and 45(3) GPa, respectively. Stilbite compressed in paraffin is characterized by $V_0 = 4426.19(17)$ Å^3 and $K_0 = 34(3)$ GPa (Fig. 4).

The behaviour of Ca-stellerite ($|Ca_{3.77}Na_{0.16}(H_2O)_{28}|$ [$Al_{7.84}Si_{28.16}O_{72}$],·Kazakovskoe deposit, Transbaikalia) at high pressure was studied earlier by single-crystal X-ray diffraction method in water (up to 1 GPa), as well as in the mixtures of methanol:ethanol 4:1 and methanol:ethanol:water 1.6:0.4:1.0 (Seryotkin et al. 2012). The PIH effect is observed in all media, evidently due to the presence of adsorbed water in alcohols. Stellerite is more compressible than stilbite, apparently because of a lesser filling of the channels.

Comparative discussion of the HP behavior of the zeolites of the heulandite group

Zeolites of STI topology belong to zeolites group with sublayered framework structure (Breck 1974; Armbruster and Gunter 2001). Besides stilbite, stellerite and barrerite, this

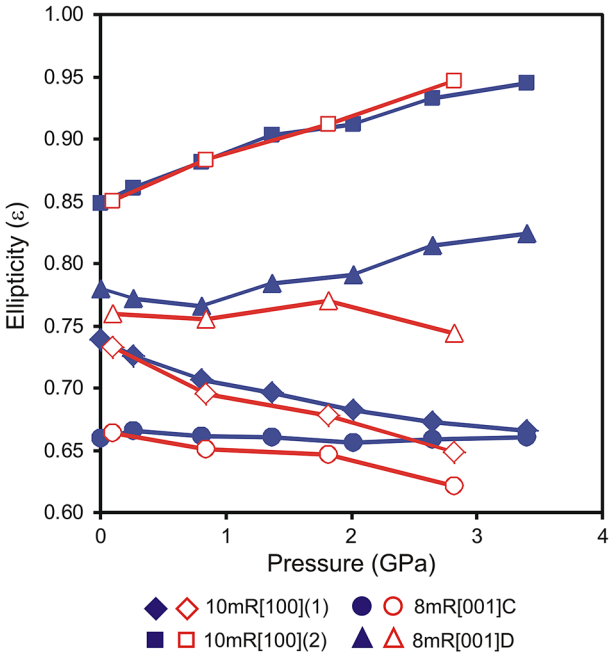

Fig. 5 The change in the ellipticity of stilbite channels during the compression in penetrating (filled symbols) and non-penetrating (open symbols) media

group includes isomorphic series heulandite–clinoptilolite, as well as brewsterite. Previously studied isostructural heulandite $Ca_{2.90}Na_{2.07}Sr_{0.25}K_{0.16}Ba_{0.06}(H_2O)_n[Al_{8.65}Si_{27.35}O_{72}]$ (Seryotkin 2015) and clinoptilolite $Ca_{1.67}Na_{2.55}K_{0.37}(H_2O)_n[Al_{6.21}Si_{29.79}O_{72}]$ (Seryotkin 2016) differ in the framework Si:Al ratio, the number and ratio of the extra-framework cations and the H_2O content. This determines also their different behaviour at high pressure. First of all, this concerns the hydration under pressure. The H_2O content in heulandite increases within a large pressure range, whereas clinoptilolite undergoes additional hydration only at the beginning of compression, and then the composition remains constant. The degree of hydration in heulandite is somewhat higher compared to clinoptilolite: on the compression in penetrating medium the H_2O content amounts to 27.4 molecules p.f.u. in heulandite and only 25.6 molecules in clinoptilolite. We can note a certain similarity in the structural evolution of zeolites belonging to stilbite–stellerite and heulandite–clinoptilolite group. Along with the increase of Al content in a compound both the pressure range of hydration and the amount of adsorbed water increase. Accordingly, the compressibility of a compound decreases, apparently due to a denser filling of the channels. This holds true for the compounds of both the STI and HEU type. Their similarity is caused, in particular, by high mobility of the H_2O molecules in their channels (Barrer and Fender 1961; Dyer and Faghihian 1998; Xu and Stebbins 1998). As concerns the third member of this group, brewsterite, it exhibits completely different behaviour under pressure. The pressure-induced changes in the structure of brewsterite pressurized in penetrating (water-containing) and non-penetrating (paraffin) media are similar, the PIH effect is absent (Seryotkin 2019). This is evidently explained by a full occupancy of the extra-framework positions and the absence of vacancies in brewsterite (Schlenker et al. 1977; Artioli et al. 1985). This, in its turn, causes low self-diffusion of H_2O molecules in its channels.

We should note that our earlier results on stellerite compression in the water-bearing medium are limited mainly to the pressure dependences of the lattice parameters. The structure of stellerite is determined only up to 0.76 GPa.

Table 5 Channel diameters (Å) and their ellipticities in framework of stilbite compressed in penetrating medium

P, GPa	0.0001	0.26	0.81	1.37	2.02	2.65	3.40
10mR[100](1)							
O1–O1	6.801 (3)	6.69 (2)	6.53 (2)	6.46 (2)	6.34 (2)	6.24 (2)	6.15 (3)
O6–O6	9.203 (5)	9.220 (13)	9.241 (13)	9.275 (14)	9.286 (16)	9.271 (18)	9.24 (2)
ε	0.7390 (8)	0.725 (3)	0.707 (3)	0.696 (3)	0.683 (3)	0.673 (4)	0.666 (5)
10mR[100](2)							
O10–O10	7.522 (3)	7.60 (2)	7.70 (2)	7.76 (2)	7.74 (2)	7.80 (2)	7.83 (3)
O6–O6	8.869 (5)	8.825 (13)	8.734 (13)	8.592 (14)	8.491 (16)	8.366 (18)	8.29 (2)
ε	0.8481 (9)	0.861 (4)	0.881 (4)	0.903 (4)	0.912 (4)	0.933 (5)	0.945 (6)
8mR[001]C							
O7–O7	5.501 (5)	5.55 (3)	5.53 (3)	5.47 (3)	5.43 (3)	5.35 (4)	5.35 (4)
O6–O6	8.340 (5)	8.336 (13)	8.352 (13)	8.284 (14)	8.265 (16)	8.124 (18)	8.10 (2)
ε	0.6596 (10)	0.665 (5)	0.662 (5)	0.660 (5)	0.657 (5)	0.659 (6)	0.661 (7)
8mR[001]D							
O6–O6	5.263 (5)	5.242 (13)	5.179 (13)	5.226 (14)	5.226 (16)	5.332 (18)	5.30 (2)
O4–O4	6.7468 (4)	6.79 (2)	6.76 (2)	6.67 (2)	6.60 (2)	6.54 (2)	6.43 (3)
ε	0.7801 (8)	0.772 (4)	0.766 (4)	0.784 (5)	0.791 (5)	0.815 (5)	0.824 (7)

Table 6 Channel diameters (Å) and their ellipticities in the framework of stilbite compressed in paraffin

P, GPa	0.10	0.84	1.82	2.82	0.0001*
10mR[100](1)					
O1–O1	6.77 (3)	6.44 (2)	6.26 (2)	6.05 (3)	6.801 (4)
O6–O6	9.229 (15)	9.254 (13)	9.233 (17)	9.32 (2)	9.210 (5)
ε	0.733 (4)	0.695 (3)	0.678 (4)	0.649 (5)	0.7384 (8)
10mR[100](2)					
O10–O10	7.54 (3)	7.67 (2)	7.76 (2)	7.87 (3)	7.524 (4)
O6–O6	8.872 (15)	8.692 (13)	8.508 (17)	8.32 (2)	8.857 (5)
ε	0.850 (4)	0.883 (4)	0.912 (4)	0.946 (7)	0.8494 (9)
8mR[001]C					
O7–O7	5.61 (4)	5.47 (3)	5.38 (3)	5.24 (5)	5.507 (5)
O6–O6	8.452 (14)	8.392 (13)	8.323 (17)	8.43 (3)	8.351 (5)
ε	0.664 (5)	0.651 (5)	0.647 (5)	0.622 (8)	0.6594 (10)
8mR[001]D					
O6–O6	5.140 (14)	5.121 (13)	5.095 (17)	4.92 (3)	5.252 (5)
O4–O4	6.76 (2)	6.78 (2)	6.61 (2)	6.61 (3)	6.754 (4)
ε	0.760 (5)	0.755 (4)	0.770 (5)	0.744 (7)	0.7776 (12)

*After decompression, in air

The compression experiments on stilbite and K,Na-stellerite (Seryotkin and Bakakin 2019) show that the filling of initially vacant water sites begins above 1 GPa. Therefore, at present we cannot assert that stellerite preserves its composition constant above 1 GPa. Additional experiments are needed to study its structural evolution up to the pressure of 4–5 GPa.

Conclusion

The single-crystal X-ray diffraction experiments in a DAC using water-bearing medium show that stilbite, containing ≈ 31 H_2O molecules per formula unit at ambient pressure, hydrates up to ≈ 34 H_2O p.f.u. in the pressure range of 0.0001–2.6 GPa. This pressure-induced hydration occurs through the additional filling of already populated water positions, as well as the filling of initially vacant sites. The compressibility of stilbite in non-penetrating fluid is higher than in the water-containing medium; above 3 GPa the structure abruptly contracts along the *b* axis with symmetry lowering to triclinic. A comparison of the results of this work with the earlier data allows to suppose that the composition of the stilbite–stellerite group minerals can also significantly influence their high-pressure behavior.

Acknowledgements This study was supported by the Russian Foundation of Basic Researches (Grant 19-05-00800) and by state assignment of IGM SB RAS.

References

Angel RJ, Gonzalez-Platas J (2013) ABSORB-7 and ABSORB-GUI for single-crystal absorption corrections. J Appl Cryst 46:252–254. https://doi.org/10.1107/S0021889812048431

Angel RJ, Gonzalez-Platas J, Alvaro M (2014) EosFit7c and a Fortran module (library) for equation of state calculations. Z Kristallogr 229:405–419. https://doi.org/10.1515/zkri-2013-1711

Arletti R, Quartieri S, Vezzalini G (2010) Elastic behavior of zeolite boggsite in silicon oil and aqueous medium: a case of high-pressure-induced over-hydration. Am Mineral 95:1247–1256. https://doi.org/10.2138/am.2010.3482

Armbruster T, Gunter ME (2001) Crystal structures of natural zeolites. In: Bish DL, Ming DW (eds) Natural zeolites. Miner Soc America, Washington, pp 1–67

Artioli G, Smith JV, Kvick Å (1985) Multiple hydrogen positions in the zeolite brewsterite, ($Sr_{0.95}$, $B_{a0.0}$5)A_l2S_i6$_{O1}$6 5$_H$2O. Acta Crystallogr C 41:492–497. https://doi.org/10.1107/S0108270185004401

Barrer RM, Fender BEF (1961) The diffusion and sorption of water in zeolites—I. Sorption. J Phys Chem Solids 21:12–24. https://doi.org/10.1016/0022-3697(61)90206-2

Boehler R (2006) New diamond cell for single-crystal X-ray diffraction. Rev Sci Instrum 77:115103. https://doi.org/10.1063/1.2372734

Breck DW (1974) Zeolite molecular sieves. John Wiley & Sons, New York

Carey JW, Bish DL (1996) Equilibrium in the clinoptilolite-H_2O system. Am Mineral 81:952–962

Drebushchak VA, Dementiev SN, SeryotkinYuV, (2012) Phase transition at thermal dehydration in stilbite. J Therm Anal Calorim 107:1293–1299. https://doi.org/10.1007/s10973-011-1608-4

Dyer A, Faghihian H (1998) Diffusion in heteroionic zeolites: part 2: diffusion of water in heteroionic stilbites. Microporous Mesoporous Mater 21:39–44. https://doi.org/10.1016/S1387-1811(97)00036-X

Fridriksson T, Bish DL, Bird DK (2003) Hydrogen-bonded water in laumontite I: X-ray powder diffraction study of water site occupancy and structural changes in laumontite during room-temperature isothermal hydration/dehydration. Am Mineral 88:277–287. https://doi.org/10.2138/am-2003-2-304

Gabuda SP, Kozlova SG (1995) Guest-guest interaction and phase transitions in the natural zeolite laumontite. J Incl Phenom Mol Recognit Chem 22:1–13. https://doi.org/10.1007/BF00706494

Galli E (1971) Refinement of the crystal structure of stilbite. Acta Crystallogr B 27:833–841. https://doi.org/10.1107/S056774087100298X

Gatta GD, Lee Y (2007) Anisotropic elastic behaviour and structural evolution of zeolite phillipsite at high pressure: a synchrotron powder diffraction study. Microporous Mesoporous Mater 105:239–250. https://doi.org/10.1016/j.micromeso.2007.01.031

Gatta GD, Lotti P, Tabacchi G (2018) The effect of pressure on open-framework silicates: elastic behaviour and crystal–fluid interaction. Phys Chem Miner 45:115–138. https://doi.org/10.1007/s00269-017-0916-z

Gottardi G, Galli E (1985) Natural zeolites. Springer-Verlag, Berlin

Koyama K, Takeuchi Y (1977) Clinoptilolite: the distribution of potassium atoms and its role in thermal stability. Z Kristallogr 145:216–239. https://doi.org/10.1524/zkri.1977.145.3-4.216

Lee Y, Hriljac JA, Vogt T, Parise JB, Artioli G (2001) First structural investigation of a super-hydrated zeolite. J Am Chem Soc 123:12732–12733. https://doi.org/10.1021/ja017098h

Lee Y, Vogt T, Hriljac JA, Parise JB, Artioli G (2002) Pressure-induced volume expansion of zeolites in the natrolite family. J Am Chem Soc 124:5466–5475. https://doi.org/10.1021/ja0255960

Lee Y, Hriljac JA, Studer A, Vogt T (2004) Anisotropic compression of edingtonite and thomsonite to 6 GPa at room temperature. Phys Chem Miner 31:22–27. https://doi.org/10.1007/s00269-003-0330-6

Likhacheva AYu, Seryotkin YuV, Manakov AYu, Goryainov SV, Ancharov AI, Sheromov MA (2007) Pressure-induced over-hydration of thomsonite: a synchrotron powder diffraction study. Am Mineral 92:1610–1615. https://doi.org/10.2138/am.2007.2566

Lotti P, Gatta GD, Merlini M, Liermann H-P (2015) High-pressure behavior of synthetic mordenite-Na: an in situ single-crystal synchrotron X-ray diffraction study. Z Kristallogr 230:201–211. https://doi.org/10.1515/zkri-2014-1796

Pabalan RT, Bertetti FP (2001) Cation-exchange properties of natural zeolites. In: Bish DL, Ming DW (eds) Natural zeolites. Miner Soc America, Washington, pp 453–518

Piermarini GJ, Block S, Barnett JD, Forman RA (1975) Calibration of the pressure dependence of the R_1 ruby fluorescence line to 195 kbar. J Appl Phys 46:2774–2780. https://doi.org/10.1063/1.321957

Quartieri S, Vezzalini G (1987) Crystal chemistry of stilbites: structure refinements of one normal and four chemically anomalous samples. Zeolites 7:163–170. https://doi.org/10.1016/0144-2449(87)90080-7

Rashchenko SV, Seryotkin YV, Bakakin VV (2012a) An X-ray single crystal study of alkaline cations influence on laumontite hydration ability: I. Humidity-induced hydration of Na,K-rich laumontite. Microporous Mesoporous Mater 151:93–98. https://doi.org/10.1016/j.micromeso.2011.11.009

Rashchenko SV, Seryotkin YV, Bakakin VV (2012b) An X-ray single-crystal study of alkaline cations influence on laumontite hydration ability: II. Pressure-induced hydration of Na, K-rich laumontite. Microporous Mesoporous Mater 159:126–131. https://doi.org/10.1016/j.micromeso.2012.04.029

Rigaku Oxford Diffraction (2016) CrysAlisPro software system. Rigaku Corporation, Oxford

Schlenker JL, Pluth JJ, Smith JV (1977) Refinement of the crystal structure of brewsterite, $Ba_{0.5}Sr_{1.5}Al_4Si_{12}O_{32}$ $10H_2O$. Acta Crystallogr B 33:2907–2910. https://doi.org/10.1107/S0567740877009765

Seryotkin YuV (2015) Influence of content of pressure-transmitting medium on structural evolution of heulandite: single-crystal X-ray diffraction study. Microporous Mesoporous Mater 214:127–135. https://doi.org/10.1016/j.micromeso.2015.05.015

Seryotkin YuV (2016) High-pressure behavior of HEU-type zeolites: X-ray diffraction study of clinoptilolite-Na. Microporous Mesoporous Mater 235:20–31. https://doi.org/10.1016/j.micromeso.2016.07.048

Seryotkin YuV (2019) Evolution of the brewsterite structure at high pressure: a single-crystal X-ray diffraction study. Microporous Mesoporous Mater 276:167–172. https://doi.org/10.1016/j.micromeso.2018.09.030

Seryotkin YuV, Bakakin VV (2019) Structure of K, Na-exchanged stellerite zeolite and its evolution under high pressure. J Struct Chem 60:1612–1621. https://doi.org/10.1134/S0022476619100068

Seryotkin YuV, Bakakin VV, Likhacheva AY, Rashchenko SV (2012) High-pressure diffraction study of zeolites stilbite and stellerite. J Struct Chem 53:26–34. https://doi.org/10.1134/S0022476612070049

Sheldrick G (2015) SHELXT–integrated space-group and crystal-structure determination. Acta Crystallogr A 71:3–8. https://doi.org/10.1107/S2053273314026370

Slaughter M (1970) Crystal structure of stilbite. Am Mineral 55:387–397

Xu Z, Stebbins JF (1998) Oxygen site exchange kinetics observed with solid state NMR in a natural zeolite. Geochim Cosmochim Acta 62:1803–1809. https://doi.org/10.1016/S0016-7037(98)00095-7